https://doi.org/10.5194/egusphere-2026-2131
Preprint. Discussion started: 28 April 2026

Seasonal icings reveal subsurface water drainage of a Greenland Ice Sheet outlet glacier

Rebecca McCerery[1], Joseph A. Graly[1], Christopher L. Hansen[2], Kate Winter[1], William P. Gilhooly III[3], Trinity L. Hamilton[2,4], Moses Jatta[3], Jeff R. Havig[2], Felipe Napoleoni[1,5], Alicia M. Rutledge[6], Matthew Terrell[3], Tanya M. Trott[7], Kayla Woodie[3], Bernd Kulessa[7], Sevi Modestou[1], Hannah Bahrani[1], Tori Kennedy[3], Alexandra Messerli[8], Kathy Licht[3]

[1]*School of Geography and Natural Sciences, Northumbria University, Newcastle-upon-Tyne, United Kingdom, NE1 8ST*

*Corresponding author rebecca.mccerery@hotmail.com

[1]School of Geography and Natural Sciences, Northumbria University, Newcastle Upon Tyne, NE1 8ST, United Kingdom

[2]Department of Plant and Microbial Biology, University of Minnesota, Saint Paul, MN 55108 USA

[3]Department of Earth & Environmental Sciences, Indiana University Indianapolis, Indianapolis, IN 46202 USA

[4]The BioTechnology Institute, University of Minnesota, Saint Paul, MN 55108 USA

[5]School of Geosciences, University of Edinburgh, Edinburgh, EH8 9XP, United Kingdom

[6]Department of Astronomy and Planetary Science, Northern Arizona University, Flagstaff, AZ 86011 USA

[7]School of Biosciences, Geography and Physics, Swansea University, Swansea, SA2 8PP, United Kingdom

[8]Asiaq Greenland Survey: Nuuk, GL

https://doi.org/10.5194/egusphere-2026-2131
Preprint. Discussion started: 28 April 2026

Abstract

In many glacial settings, winter outflows of proglacial water create stratified domed ice structures on glacial forefields. These structures, called naledi, provide an opportunity to characterise the solute fluxes of hydrological systems in winter which are poorly constrained compared to summer outflows which are dominated by supraglacial meltwater input. To characterise the different hydrological systems feeding naledi and provide conceptual models of their formation, we sampled 12 overwinter naledi and 4 supercooled summer ice accumulations (accreted ice) from the forefield of Isunnguata Sermia, a western outlet glacier of the Greenland Ice Sheet, during four field campaigns. Major ions and stable water isotopes reveal complex geochemical signatures, where the composition of successive naled layers reveal fluctuations in water source and transport throughout winter. In comparison, core analysis of summer accreted ice shows uniform geochemistry throughout, suggesting freeze-on of water from one single source in quick discrete events. These findings are supported by Electrical Resistivity Tomography (ERT) geophysical surveys, which reveal shallow hydrological pathways (1 – 5 m below the surface) in the glacial foreland (surveyed 400 m from the glacier terminus). Here, meltwater is transported through a saturated sediment zone feeding proglacial upwellings. Our results inform the first conceptual models of summer vs. wintertime subglacial water routing and naled formation in the proglacial zone of the Greenland Ice Sheet. We show that wintertime naledi form from a combination of top-down (unconfined) and bottom-up (confined) freezing processes which incorporates subglacial discharge, overland flow and precipitation, whereas accreted ice forms from upwellings of high velocity, highly pressurised water which freezes upon release. These seasonal changes drive different geochemical and nutrient outputs, which are critical for evaluating glacier meltwater contributions to proglacial groundwater systems and the impact of glacial discharge on downstream ecosystems.

https://doi.org/10.5194/egusphere-2026-2131
Preprint. Discussion started: 28 April 2026

1. Introduction

The Greenland Ice Sheet is a major exporter of biologically important elements to the world's oceans (Hawkings et al., 2016; Lawson et al., 2014; Wadham et al., 2016) and a hotspot for CO_2 drawdown through chemical weathering processes (Graly et al., 2017a; Pain et al., 2021). Most of our knowledge of chemical and biological fluxes from the Greenland Ice Sheet come from analysis of the summer ablation season outflow, where channelised melt waters contact only a limited portion of the glacier bed (Bhatia et al., 2013; Hawkings et al., 2016; Jacob et al., 2014; Meire et al., 2016; Yde et al., 2014). However, during winter, outflow is more typically fed by slower-flowing subglacial meltwater, which has often been subjected to greater contact time with the ice/bed interface (Chandler et al., 2013; Davison et al., 2019). As there are inherent challenges associated with field sampling subglacial water flow over winter, there is limited inclusion of winter water in geochemical modelling, inhibiting our understanding of year-round subglacial weathering processes and nutrient export from Greenland.

In many proglacial environments in the Arctic, domed ice structures called naledi (singular *naled*, but also referred to as *aufeis* or *icings*) develop within glacier forefields in the winter months (Carey, 1973; Hodgkins et al., 2004; Mallinson et al., 2019; Morse and Wolfe, 2015; Sobota, 2016; Yoshikawa et al., 2007). These naledi typically consist of stratified layers of frozen subsurface and subglacial water that has been discharged over winter (November - March). As such, they provide a potential source for characterising wintertime solute fluxes and chemical weathering processes operating over low-flow hydrological conditions that are difficult to obtain by other means. Layers build up over winter to produce a domed, layered, ice structure, which can reach multi-metre heights, forming where outflows of water are expelled in discrete locations of the glacial foreland and quickly freeze due to low air temperatures (Harden et al., 1977; Kane, 1981).

https://doi.org/10.5194/egusphere-2026-2131
Preprint. Discussion started: 28 April 2026

The prevailing theoretical models of naled formation, established ~40 years ago, suggest that naled grow in a top-down fashion because the cold winter atmosphere acts as a heat sink, freezing unconfined waters (meltwater or snow) that accumulate from above (Fig. 1a-c) (Schohl and Ettema, 1986; Yde et al., 2012). However, more recent and direct observations of proglacial naled in Svalbard by Stachnik et al. (2016) interpreted naled formation as a primarily bottom-up process. This theory suggests new meltwaters confined below ice push up older, frozen layers (Fig. 1d-f), and that liquid water conduits within naled ice provide insulated transport pathways, protected from the cold surface (Fig. 1f). These contrasting models of formation make it challenging to extrapolate general chemical and biological insights into different hydrological systems.

In previous research, principally on Svalbard, the chemistry preserved in naled ice has been successfully characterised by analysing ice cores collected in early spring (Stachnik et al., 2016; Wadham et al., 2000; Yde et al., 2012). These studies found that the overwinter solute flux captured in naled differ significantly from the early spring or late summer meltwater output from glacial systems, suggesting they can capture a distinct wintertime hydrochemical regime (Graly et al., 2018). However, complexity in their geochemistry indicates multiple water source inputs may build up a single naled (Yde et al., 2012) with chemical differences between different ice layers (Stachnik et al., 2016). The glaciers of Svalbard represent relatively small glacier hydrologic systems, with small storage capacities compared to larger ice sheets, like the Greenland Ice Sheet and its outlet glaciers (Wadham et al., 2000). It is therefore possible that the chemical signatures of naled ice in these larger systems may represent different formation mechanisms than those in Svalbard. In glacial foreland areas, supercooled waters can also freeze and build up accreted ice structures over summer, often during high discharge events sourced from glacial overdeepenings that are heavily sediment-laden (Alley et al., 1998;

https://doi.org/10.5194/egusphere-2026-2131
Preprint. Discussion started: 28 April 2026

95 Evenson et al., 1999; Lawson et al., 1998; Roberts et al., 2001; Roberts et al., 2002; Livingstone
96 et al., 2026).

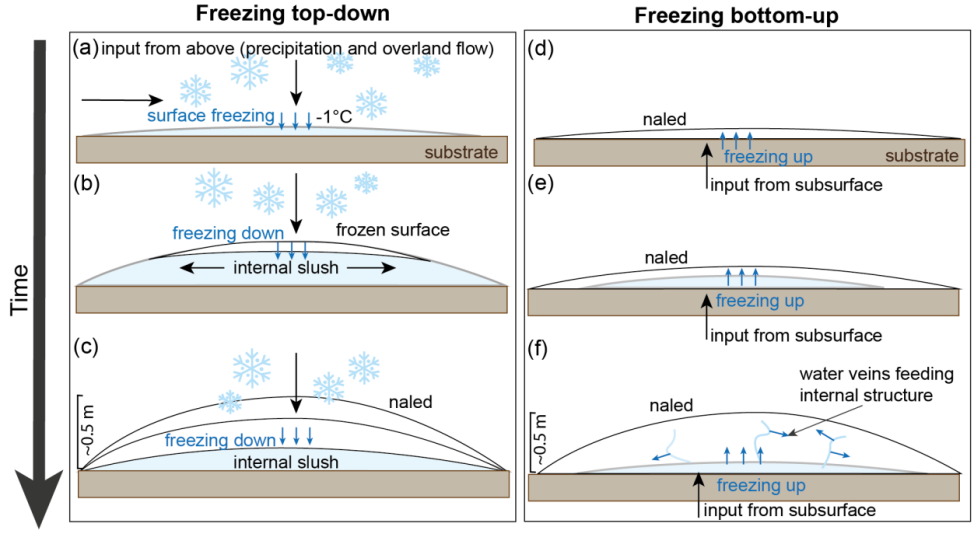

97

98 **Figure 1** Prevailing theories of naled ice formation. (a-c) A top-down freezing process by
99 which overland flow and precipitation freeze at the surface due to subzero air temperatures
100 (Schohl and Ettema, 1986). (d-f) A bottom-up freezing process by which subsurface waters
101 erupt into the forefield and freeze from the base-up, with newly erupting waters accreting onto
102 the bottom of the naled. In these bottom-up models there is also potential for small water veins
103 within the naled to accrete ice within (Wadham et al., 2000; Stachnik et al., 2016).
104

105 Here, we measure and interpret the chemical characteristics and identify the sources of
106 water creating wintertime naled ice and summertime accreted ice in the forefield of Isunnguata
107 Sermia on the western Greenland Ice Sheet, to explore seasonal changes in the hydrological
108 system. We combine our geochemical analyses with geophysical surveys of the forefield to
109 assess potential routing mechanisms of water flow, feeding these structures. Our results inform
110 a new conceptual model of naled and accreted ice formation and has applications for spatial
111 and temporal analysis of similar proglacial systems and subglacial processes in West Greenland
112 and other glaciated regions.

https://doi.org/10.5194/egusphere-2026-2131
Preprint. Discussion started: 28 April 2026

2. Study site

Isunnguata Sermia (N67.1850, W-50.3394) drains ~15,900 km^2 of the Greenland Ice Sheet and is located approximately 100 km away from the coast (Fig. 2) (Lindbäck et al., 2015). It is located in the central west region of Greenland, where ice is routed through an overdeepened bed (extending to ~350 m below sea level) for over 20 km (Lindbäck et al., 2015). Throughout its catchment area, Isunnguata Sermia is expected to flow over granodioritic gneisses and associated silicate rocks of the Nassuttooqidian Orogen, a large-scale fold-belt formed c. 2.7 billion years ago (van Gool et al., 2002).

Previous work has characterised spring/summer runoff and subglacial hydrology at Isunnguata Sermia (Bartholomew et al., 2011; Meierbachtol et al., 2013) as well as subglacial discharge and hydrochemistry of summer outflows (Graly et al., 2017a). Wintertime outflow was chemically profiled by Pitcher et al. (2020), who sampled proglacial river water while performing local radar surveys of Isunnguata Sermia. This revealed that basal water is persistent at Isunnguata Sermia, discharging small amounts of water into the proglacial river system year-round. Isunnguata Sermia also sits on a reverse gradient bed slope with an active subglacial lake system (Livingstone et al., 2019). These lakes, located beneath the ablation zone of Isunnguata Sermia have been shown to exhibit multi-year water storage, resulting in long water residence times, though research has also shown that meltwater can be quickly released during flood events (Chu et al., 2016; Livingstone et al., 2019).

The forefield of Isunnguata Sermia contains several discreet upwellings of subglacial water. These waters may emerge slowly, or as geyser-like features that expel water into the air on a meter to multi-meter scale (Livingstone et al., 2026). In February 2015, supercooled water was discovered below the clear ice of a proglacial outlet stream, 1 km downstream of the Isunnguata Sermia terminus (Pitcher et al., 2020). This slow meltwater drainage, fed by the deeply incised subglacial trough that extends inland from the terminus (Graly et al., 2017a),

https://doi.org/10.5194/egusphere-2026-2131
Preprint. Discussion started: 28 April 2026

suggests that the local geometry might drive proglacial upwellings of subglacial meltwater year-round. As a result, this site provides an ideal location to investigate the geochemical signature of water sources feeding naled ice and accreted ice, allowing us to examine changes in hydrological pathways and fully characterise the chemical signature of year-round outflows, for the first time.

3. Methods

3.1. Automatic cameras

Monitoring of glacier outflow and the development of naledi were performed by setting up timelapse cameras (LTL-6210MC Plus Scouting Cameras) at six locations across the glacier forefield over winter in 2022 and 2023 (Fig. 2 and Table S1). Cameras were set up at various locations and orientations to capture changes in the main outflow channel of Isunnguata Sermia and to review active upwellings at the time of installation. Photographs were taken at 11am, 12pm, 1pm and 2pm (local time) each day.

3.2. Sampling

Four field campaigns were conducted with the aim of collecting a representative sample set of ice and water samples across the Isunnguata Sermia forefield over multiple years both pre- and post-melt season (Fig. 2). We focused on three different sample types (i) naled ice (dome shaped structures, formed over winter likely during low discharge), (ii) naled waters upwelling in the outwash plain (capturing active water sources feeding naled ice over the winter months) and (iii) accreted ice (sediment-laden ice structures associated with active upwellings in the summer months) (Fig. 2).

Over the course of four field campaigns (October 2022, March-April 2023 September 2023 and March-April 2024) we sampled 12 naledi and four accreted ice structures (Fig 2a, Fig. S1 and 2). Ice cores were extracted with a motorised SIPRE Auger to a maximum depth

https://doi.org/10.5194/egusphere-2026-2131
Preprint. Discussion started: 28 April 2026

of 2 m. Cores were logged immediately, then sectioned by changes in ice facies and transported in individual sterile Whirl-Pak bags (Fig. 3). Core sections were then melted in a gently heated water bath in the field (less than 4 hours after sampling). The resultant waters were filtered using Whatman 0.45µm cellulose membrane filters, before being decanted into centrifuge tubes for major ion analysis. All samples were refrigerated and stored at 3-4°C until analysis. Four of the naled ice cores terminated in water sources. Cores at the other seven sites did not reach water and were limited to depths of between 8 and 139 cm often due to the presence of thick gravel beds, which rendered further drilling impossible.

Of the cores that reached active water sources, naled I8 was located at the margin of the main meltwater channel and the three others (I2, I3 and I10) in an adjacent lateral meltwater stream (Fig. 2). In each case, samples of the naled upwelling waters were collected in sterile 50 ml centrifuge tubes and filtered using Whatman 0.45µm nylon membrane filters. Accreted ice cores were sampled around the glacier front and within the main active frozen meltwater channel area in October 2022 (n = 4, Fig. 2a, Fig. 4 and Fig. S3). Unlike the naled ice core sites, none of the accreted ice cores reached free-flowing waters. Cores were described, sectioned, melted and filtered in the same manner as described above.

https://doi.org/10.5194/egusphere-2026-2131
Preprint. Discussion started: 28 April 2026

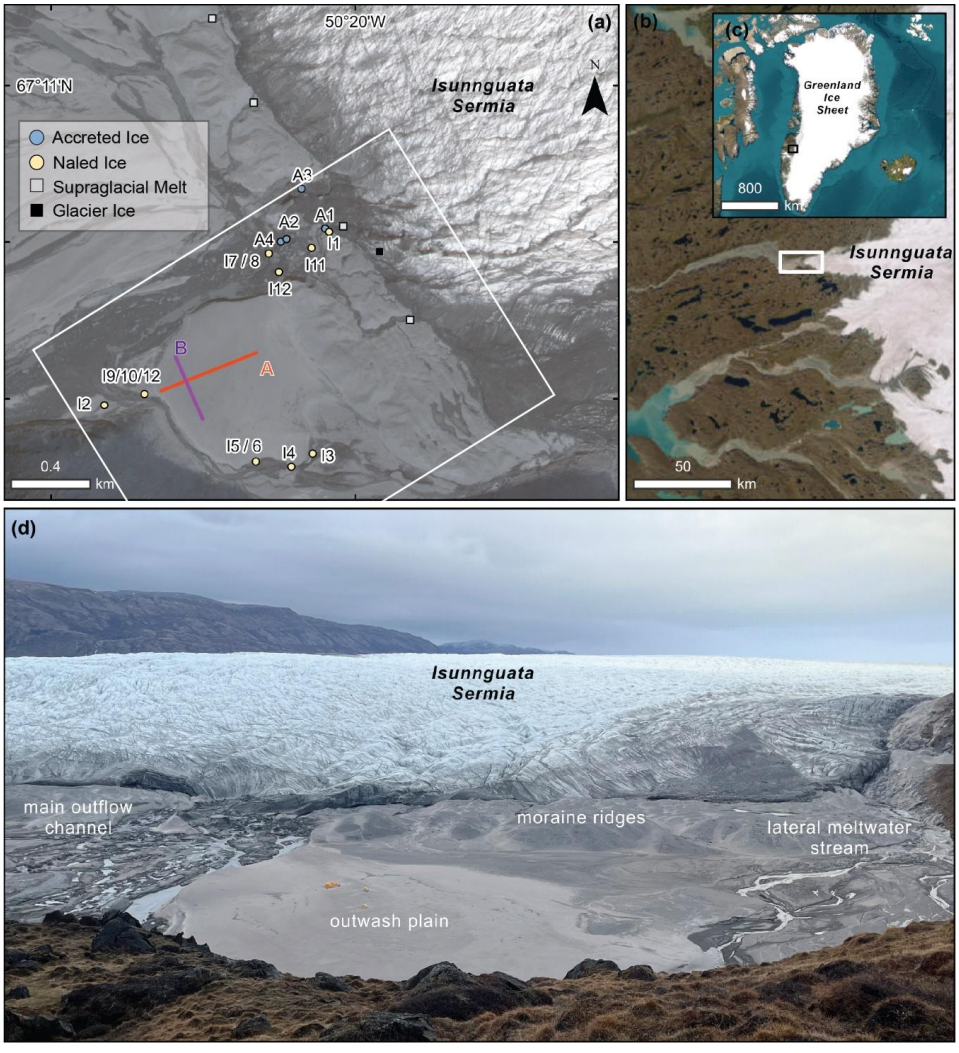

Figure 2. Isunnguata Semia field site in West Greenland (a) Location of sampling sites, geophysical survey transects (A and B) and camera trap locations in the forefield of Isunnguata Sermia. White box denotes the photograph area shown in (d). (b) Sample area of the Isunnguata Sermia forefield (white box), where meltwater is exported from the Greenland Ice Sheet (c). (d) Overview photograph of the proglacial forefield from May 2023 with key sites annotated. The yellow features on the outwash plain are camp tents, which are approximately 1.6 to 1.9 meters high. Satellite images in panel a sourced from the Polar Geospatial Centre (from June 2022) and panels b-c Sources: Esri basemap imagery | Powered by Esri.

https://doi.org/10.5194/egusphere-2026-2131
Preprint. Discussion started: 28 April 2026

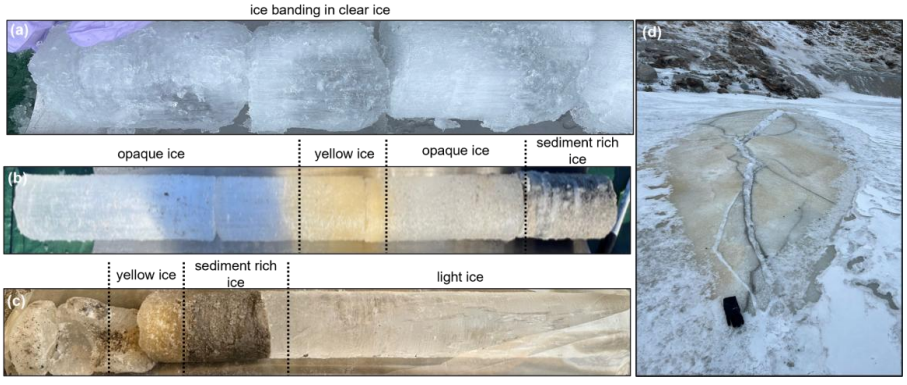

Figure 3 Naled ice structures. Examples of different ice facies from cores drilled through naled ice structures (a) core I3 (15 cm) (b) upper 90 cm of core I10 and (c) lower 68 cm of core I10, as well as a photograph of a naled structure (cored for I10) (d) where a black glove (~20 cm in length) is provided for scale.

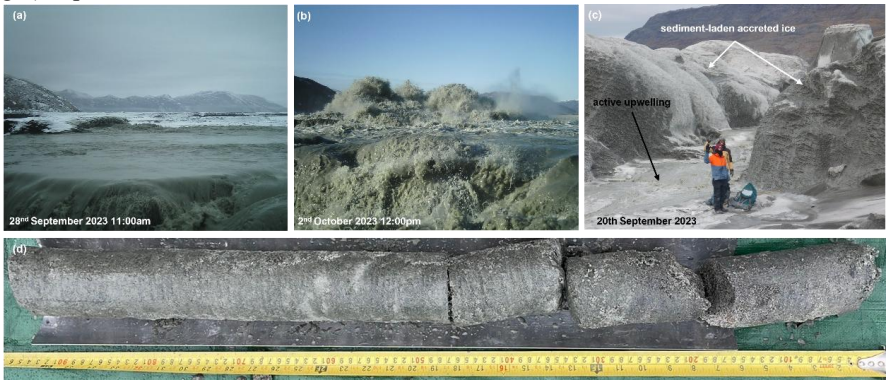

Figure 4 (a-b) Examples of a subglacial water outburst from Isunnguata Sermia, captured by automatic camera 4 in late September to early October 2023. High water flow volumes on the 28th of September (a) were followed by erupting outflow just 4 days later (b). (c) Example of a multi-metre scale accreted ice structure, captures on the 20th of September 2023, showing an active, bubbling upwelling of water in the forefield of Isunnguata Sermia, where accreted ice (~2 m high) has built up to the sides of the upwelling. (d) Example of an ice core from an accreted ice structure, rich in sediment.

Contextual samples of glacier ice (n = 1) and supraglacial meltwater (n = 4) were also collected to represent end member water types. Glacier ice was sampled from the upper ice margin of Isunnguata Sermia in April 2024 (Fig. 2a). Ice was extracted via a chisel and hammer with the upper 10 cm layer of ice discarded so that less weathered ice could be sampled.

https://doi.org/10.5194/egusphere-2026-2131
Preprint. Discussion started: 28 April 2026

Supraglacial water was sampled from the ice margin and atop the Isunnguata Sermia glacier snout in 50 ml centrifuge tubes.

3.3. Geochemistry

Concentrations of major anions in water and melted ice samples were analysed in triplicate on a Dionex Integrion high-pressure ion chromatography (HPIC) system at Northumbria University using 5 ml of sample. Standard solutions of fluoride (F^-), chloride (Cl^-), sulphate (SO_4^{2-}), and nitrate (NO_3^-) were prepared using 18.2 MΩ ultrapure water to obtain standard curves. Concentrations of major cations were analysed in triplicate on an Optima 8000 inductively coupled plasma optical emission spectrometer (ICP-OES) at Northumbria University using 7 ml of sample. Standard solutions of calcium (Ca), potassium (K), magnesium (Mg), and sodium (Na) were prepared using ultrapure water to obtain standard curves. HCO_3^- was calculated using the charge balance error (CBE) method, determined by Equation 1 where ε^+ and ε^- are total cation and anion equivalents:

$$CBE = \frac{(\varepsilon^+ - \varepsilon^-)}{(\varepsilon^+ + \varepsilon^-)} x100 \quad \text{(Eq. 1)}$$

3.4. Stable water isotopes

Aliquots from melted cores and water samples were analysed for their hydrogen and oxygen isotopic composition using a Picarro L2130-i cavity ringdown spectrometer at Northumbria University. Four calibration standards were measured at the beginning of each run (including in-house laboratory standards supplied and calibrated by the University of Bergen ('EVAP-2', 'FINSE', 'GLW') and international standard SLAP2 (Standard Light Antarctic Precipitation 2). Separate aliquots of reference water 'Medium Natural Water ' or 'Greenland Water' (purchased from Elemental Microanalysis Ltd.) were interspersed approximately every 10-15

https://doi.org/10.5194/egusphere-2026-2131
Preprint. Discussion started: 28 April 2026

samples and used to monitor and correct instrument drift. Results were corrected for memory and drift and normalised to the VSMOW-SLAP (Vienna Standard Mean Ocean Water – Standard Light Antarctic Precipitation) scale, using the FARLAB Liquid Water Isotope Measurement Processor (FLIIMP) software package (Sodemann et al., 2023). No humidity correction was applied (following Weng et al., 2020). The drift standards (as well as one aliquot of VSMOW2 per run) were also used as data quality monitors. Analytical error is equal to or better than 0.4‰ for δD and 0.07‰ for $\delta^{18}O$ (SE); overall reproducibility based on monitor standards is equal to or better than 1.0‰ for δD, and 0.38‰ on $\delta^{18}O$ (SD) (Table S2). Individual 'freezing packages' which are discrete isotopic units within the naled ice body representing a temporally distinct episode of water upwelling and subsequent freezing at the ice surface were also identified by calculating freezing-curves for each ice core. In the context of refreezing Greenland Ice Sheet waters, a δD:$\delta^{18}O$ slope of around 6 is expected. The composition of the source water can be calculated from the two-isotope slope (Souchez and Jouzel, 1984), allowing us to determine the isotopic composition of the source water where a freezing slope is identified.

3.5. Electrical Resistivity Tomography

A SuperSting R8 eight-channel earth resistivity meter (Advanced Geosciences, Inc.), was used to investigate subsurface conditions and potential water transport routes through the forefield of Isunnguata Sermia (Fig. 2) in April 2024. Prior to deployment, the frozen ground had to be prepared for electrode stake deployment. For each stake, small areas of frozen ground were thawed to a depth of ~30 cm using boiled water, heated from locally sourced snowmelt. A mixture of locally sourced glacial clay and salt or isotonic powder (Gatorade™) was poured over the thawed ground to secure each electrode stake and ensure sufficient ground coupling once the electrodes froze in. Fifty-six electrodes were installed in a forward and reverse

https://doi.org/10.5194/egusphere-2026-2131
Preprint. Discussion started: 28 April 2026

dipole-dipole configuration along profile A with the same configuration along profile B (Fig. 2), where 47 electrodes were placed. The maximum source current was set to 50 mA for both profiles and electrode contact resistance was monitored throughout. All data were processed and inverted using ResIPy v3.6.3 (Blanchy et al., 2020). The full data processing methodology is available in the Supplementary Information.

4. Results

4.1. Automatic cameras and Field Photos

The automatic cameras were set up with the aim of recording the development of naled ice (full descriptions of camera traps and observations can be found in Supplementary Information Table S1). Cameras captured active naled formation as well as changes in winter outflow over the foreland of Isunnguata Sermia. Camera 5, for example, captured an outflow of yellow-coloured water on the 22nd of October 2023 (shown in Fig. 5). The origins of this yellow water flow are not fully clear and may originate from a location off-camera or from the rising domed naled structure; but its distinct colouration dominated for over 3 days, where layers of yellow-coloured ice seemed to build up from the margins of the outflow, before being covered by fresh snow on 28th October. This created a clear ice layer on top of the yellow covered ice. These accumulation patterns, recorded for the first time by our automatic cameras suggest that similar ice layering may be expected in naled formations, and the ice cores extracted from them. This camera also captured the formation of winter-accumulating naled ice in the distance (Fig 5).

A glacial outburst flood from Isunnguata Sermia was detected between September and early October 2023 (Livingstone et al. 2026). By analysing footage from two separate automatic cameras, placed in different locations, facing different orientations (see Supplementary Information) we can see a gradual increase in water levels of the main meltwater channel, before a vigorous outburst flood event occurred on October 2nd (Fig. 4a-b).

https://doi.org/10.5194/egusphere-2026-2131
Preprint. Discussion started: 28 April 2026

Figure 5 Upwelling of glacial waters in the forefield of Isunnguata Sermia, captured by an automatic camera installation (Camera 5) - installed for the 2023/2024 winter season (a-d). Over the course of 6 days, distinctly yellow-coloured water flows and ice accumulations were recorded, suggesting variable water/snow inputs/throughputs. (a) Photograph showing the first emergence of yellow-coloured water in the glacial foreland. (b) The yellow outflow completely covers the proglacial river in the field of view. (c) White ice and snow begin to overlay the yellow layer which have frozen. (d) The yellow ice layer is fully covered with fresh white ice and snow. Black dashed outline highlights the naled ice area. (e) A naled dome formed in the centre of the proglacial stream overnight on the 2nd April 2024 captured in field photographs.

https://doi.org/10.5194/egusphere-2026-2131
Preprint. Discussion started: 28 April 2026

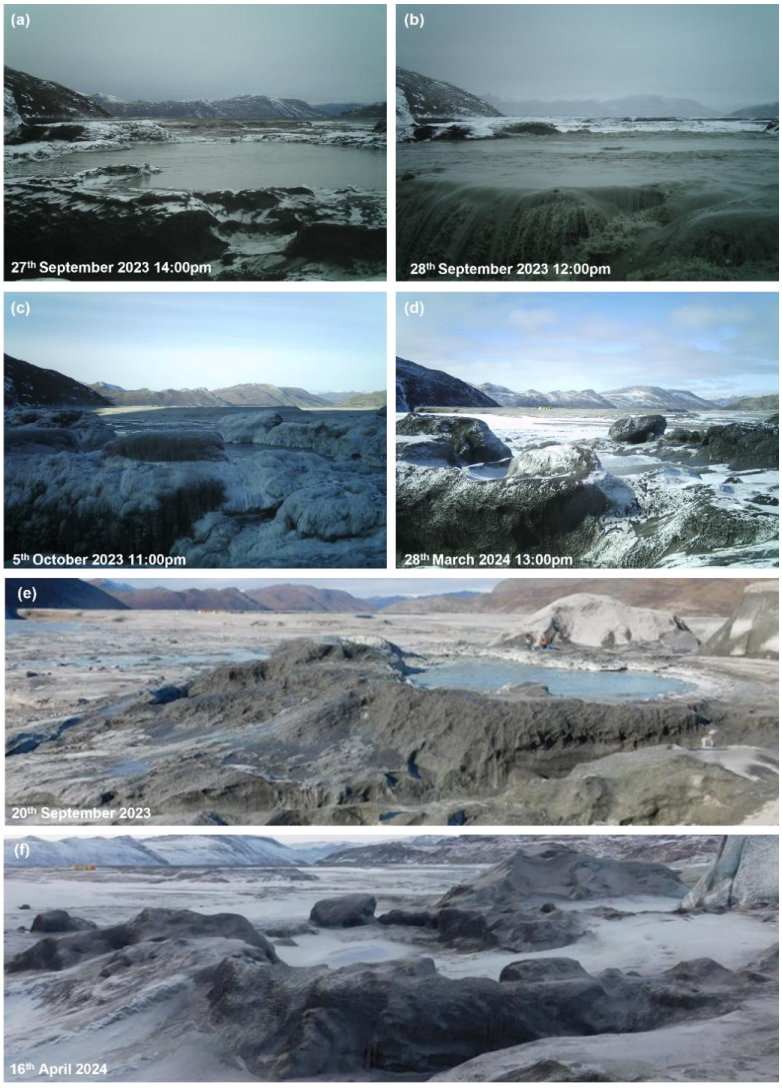

Figure 6 Accreted ice formation (a-d) captured by an automatic camera installation - installed for the 2023/2024 winter season. (a-b) Over the course of a week towards the end of the melt season, an eruption of glacial meltwater occurred in the main proglacial meltwater channel close to the Isunnguata Sermia ice margin (Livingstone et al., 2026), see - https://vimeo.com/manage/videos/1103612163 (c) This resulted in the rapid accumulation of ice accretions around the source of the upwelling. (d) Over 6 months later, some of that ice accumulation persists around the upwelling source, likely preserved by the cold winter temperatures though the ice structure appears deflated and eroded suggesting some melt wastage has begun to occur. A similar process is seen in (e) where sediment-rich ice accumulations around an upwelling site in late September 2023 had delated and eroded substantially (f) the following April 2024.

https://doi.org/10.5194/egusphere-2026-2131
Preprint. Discussion started: 28 April 2026

4.2. Ice facies analysis

Ice cores revealed distinct ice facies, which we group into four classifications: light ice, opaque ice, yellow-coloured ice, and sediment-rich ice (Fig. 3). Some ice has either horizontal or vertical stripes – which are more visible in the 'light ice' and 'opaque ice'. Light ice and opaque ice packages do not have sediment inclusions or discolouration. Light ice was mostly translucent, whereas opaque ice appeared white or 'clouded', both ice types were combined together for geochemical analysis as 'clear ice' for simplicity. Yellow-coloured ice was distinctly yellow in colour and appeared as discrete layers within the naled cores. Five ice cores recorded these yellow-coloured ice layers which ranged in thickness from 10-25 cm, at various depths (Fig. 7b, e; Fig. 8a, c, e). Yellow-coloured ice did not appear in the accreted ice cores. Sediment-rich ice had clear sediment inclusions that accounted for >50% of the core section. Sediment layers were present in nearly all core samples (except I2, I7 and I8), with more pronounced sediment-rich layers (between 10-40 cm thick) recorded in I1, I3, I5 and I10 (Fig. 7 and 8). These sediment-rich layers only appeared as discrete layers within the naled cores but they account for almost the full core length in the accreted ice cores (Fig. 3 and 4). Facies logs for each ice core and their resultant geochemical profiles are provided in Figures 7, 8 and 9.

Accreted ice cores were typically multi-metre in length and consisted of heavily sediment-laden ice (Fig. 4). This ice appears to be a mix of frazil ice and silt to fine sand sediments and cores range in length from ~25 to 240 cm (Fig. 9). The longest core, A4, had no visible layers, but the full core was sediment-laden with clay to fine sand sized particles (see Fig. 4d). Bands of opaque ice, less than 10 cm thick were recorded at various intervals throughout cores A1, A2 and A3. Aside from these intersections, all accreted ice cores exhibit similar sediment-laden ice facies with tabular ice lenses (Fig. 4) and limited discernible differences between and within ice cores.

https://doi.org/10.5194/egusphere-2026-2131
Preprint. Discussion started: 28 April 2026

4.3. Geochemistry

Proportions of major ions and total dissolved solids (TDS) are shown for each core in Fig. 7, 8 and 9. The naled ice cores display a range of total dissolved solids (TDS) concentrations, broadly spanning from very dilute (less than 1 mg L^{-1}) to highly concentrated (up to 1,300 mg L^{-1}) depending on the core and depth. Across most cores, HCO_3^- is the dominant anion, while Ca^{2+} is consistently the most abundant cation. In general, we observe that ice layers with low TDS, such as those found throughout naled I1 and the lower portions of I7 (Fig. 7a. Fig. 8b), are typically SO_4^{2-} poor (though sometimes NO_3^- enriched), and very concentrated TDS layers such as the naled waters in I2 and I3 (Fig.7b and c) are more often SO_4^{2-} enriched. Naled waters from I2 and I3, exhibit substantially higher TDS concentrations than the overlying ice. The geochemical composition of some of the naled waters are not represented in Fig.8, namely cores I8 and I10, as an unknown source of positive charge was detected causing a large change imbalance.

In terms of spatial differences, naled I1 was unique in that it was extracted from beneath a layer of mud whereas all other naled icings were collected from clean ice surfaces. The upper layer of naled I1 with some sediment inclusions, had no detectable SO_4^{2-} and low TDS values of 2.5 mg L^{-1} (Fig. 7a) Naled I1 was also the naled structure closest to the glacier margin and located in the main meltwater channel. Similarly, naled I7 and I8 (two samples taken from the same naled structure, Fig. 2a) and I11 were also located in the main channel. I12 was then sampled as a newly emerging naled with only a thin layer of domed ice extracted after it was observed to have begun forming in the main channel overnight in March 2024. Here, the very surface of the naled ice was sampled and showed moderate TDS amounts of 16-18 mg L^{-1} with an almost even proportion of HCO_3^- and SO_4^{2-}, similar to the ion proportions seen in other naled ice cores (Fig. 9b). All of the cores sampled from the main channel lack yellow ice layers within the naled cores apart from I8 with a distinct yellow layer at the very surface and yellow

https://doi.org/10.5194/egusphere-2026-2131
Preprint. Discussion started: 28 April 2026

348 water at the base of the core (Fig. 8). These main channel cores generally exhibit moderate
349 TDS concentrations, with the exception of I8 which reaches up to 140 mg L^{-1} at its base. HCO_3^-
350 dominance is consistent across all main channel cores, SO_4^{2-} contributions remain relatively
351 low compared to some side channel cores. NO_3^- is slightly more elevated in I8 than in the other
352 main channel cores.

353 Side channel cores, I2, I3, I4, I5, I6, I9 and I10 show greater variability in both TDS
354 amounts (1-500 mg L^{-1} in ice and 1,300 mg L^{-1} in naled waters) and ion proportions. While
355 HCO_3^- and Ca^{2+} still dominate in many of these cores, SO_4^{2-} contributes more the proportion
356 of ions across several of them, most notably the naled water in I2, I6, and I10. Core I10 is
357 particularly distinct, with SO_4^{2-} comprising over 40% of total ions throughout and TDS values
358 reaching up to 500 mg L^{-1} in the yellow ice layers. Naled waters sampled beneath I2 and I3
359 also show substantially higher TDS concentrations of 1,300 mg L^{-1} and 890 mg L^{-1}
360 respectively.

361 Accreted ice cores (A1-A4) are much more uniform than naled ice cores in their
362 geochemical signature both within single cores and across cores (Fig. 9c-f). All cores have
363 TDS concentrations between 7-30 mg L^{-1} (Fig. 9c-f). HCO_3^- and Ca^{2+} consistently dominate
364 throughout all of cores at 50-80% of anions and cations respectively. The most variability is
365 seen in accreted core A4 where SO_4^- dominates the anions in some of the core sections.
366 Accreted cores also have marginally higher proportions of K^+ compared to the naled ice cores.

https://doi.org/10.5194/egusphere-2026-2131
Preprint. Discussion started: 28 April 2026

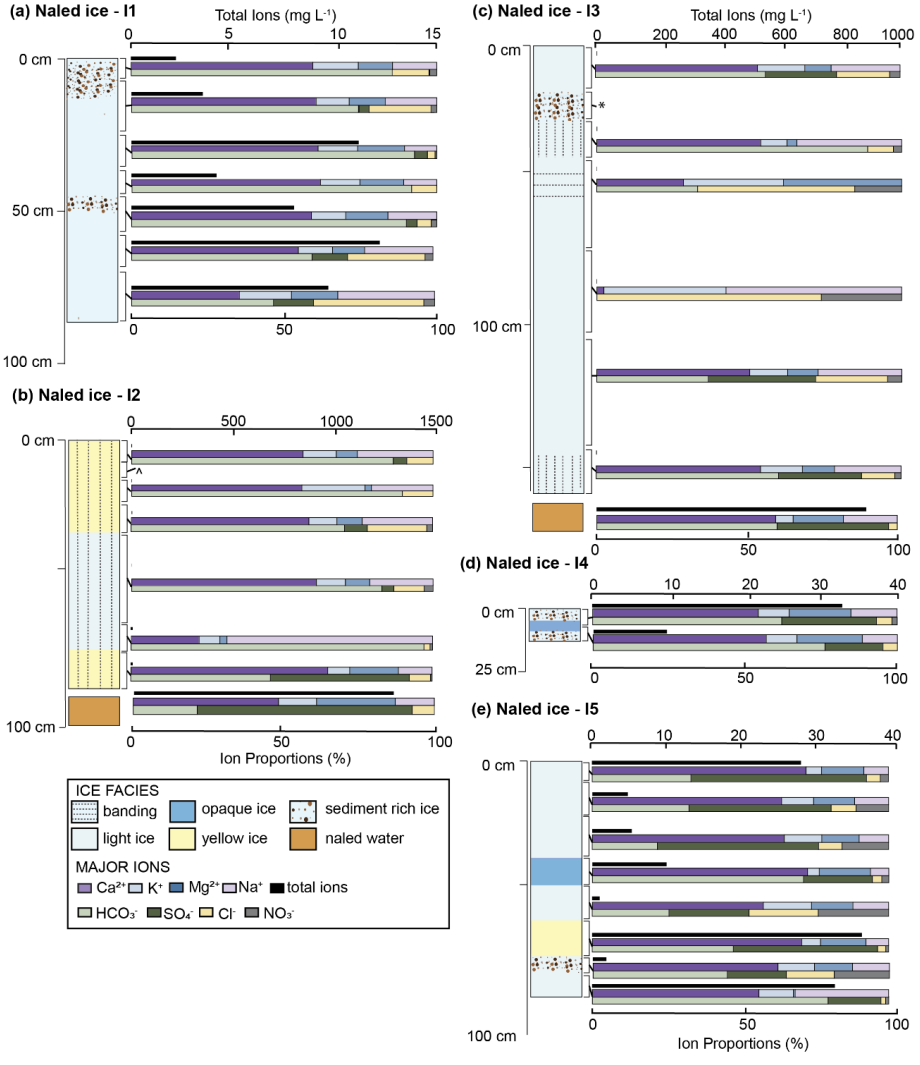

367

368 **Figure** 7 Ice facies and geochemical profiles of major ions for naled ice cores I1 through
369 I5 collected April 2023 and March-April 2024. Vertical columns indicate ice facies types.
370 Geochemical results are illustrated with cumulative horizontal bars adjacent to sampling
371 depth (exact depth range indicated by black brackets). Total dissolved solids (TDS) are
372 given in mg L^{-1} (upper, black bar); note unique axis values for each core. For some
373 samples, values are so low, they plot as a point. The proportions of cations (middle bar
374 plot, Ca^{2+}, K^{+}, Mg^{2+}, and Na^{+}) and anions (lower bar plot, Cl^{-}, SO_4^{2-}, NO_3^{-}, and HCO_3^{-}).

https://doi.org/10.5194/egusphere-2026-2131
Preprint. Discussion started: 28 April 2026

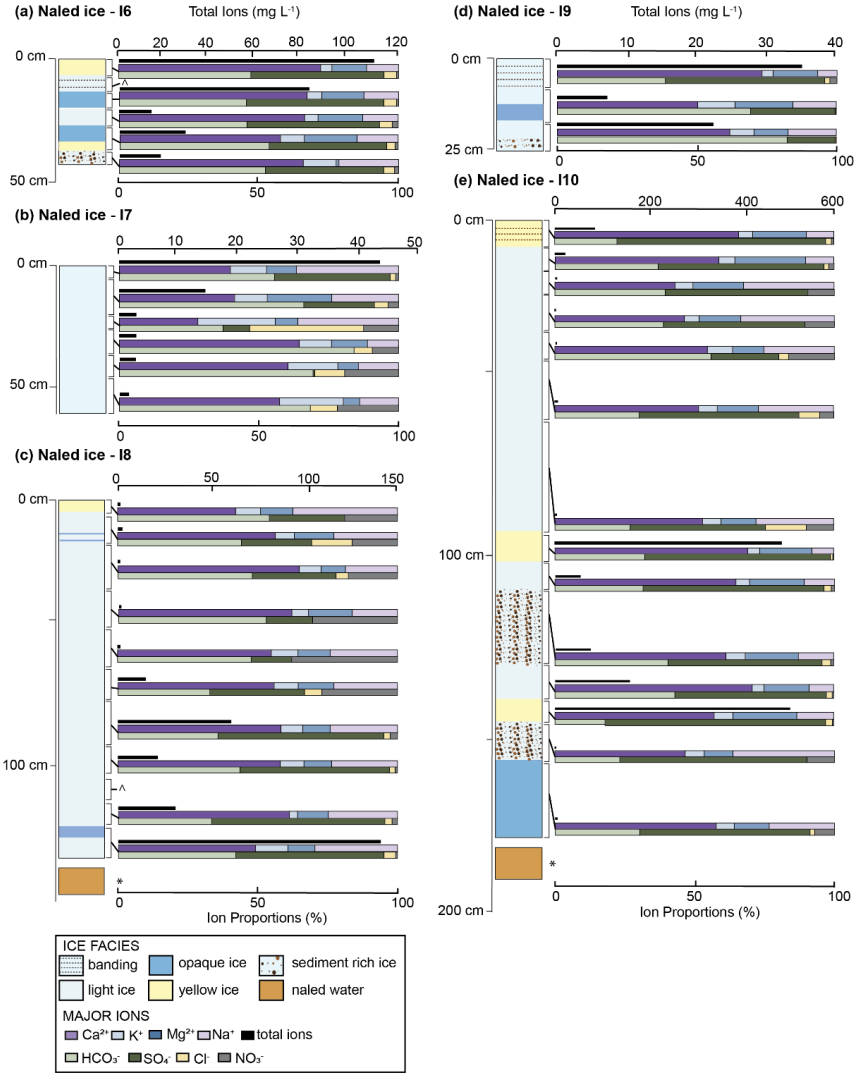

375

376 **Figure 8** Ice facies and geochemical profile of major ions for naled ice cores I6 through
377 I10 collected March-April 2024. Vertical columns indicate ice facies types and changes
378 with depth. Geochemical results are illustrated with cumulative horizontal bars adjacent
379 to sampling depth (exact depth range indicated by black brackets). TDS is given in mg L^{-1}
380 (upper bar; note unique charge range for each core) and the proportions cations (middle
381 bar plot, Ca^{2+}, K^{+}, Mg^{2+}, and Na^{+}) and anions (lower bar plot, Cl^{-}, SO_4^{2-}, NO^{3-}, and HCO_3^{-}
382). *Naled water in core I8 and I10 has an unknown source of positive charge and is
383 therefore not included in the graph. ^Sample not analysed.

https://doi.org/10.5194/egusphere-2026-2131
Preprint. Discussion started: 28 April 2026

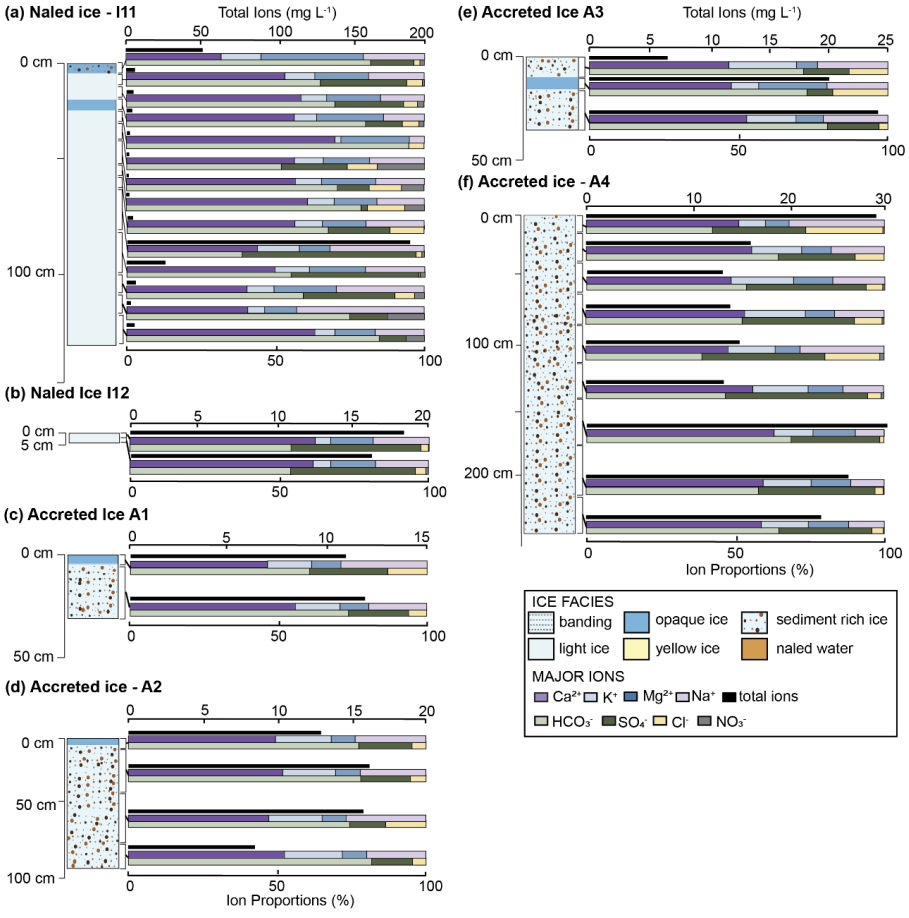

Figure 9 Ice facies and geochemical profile of major ions for naled ice cores I11 and I12 collected March-April 2024 and accreted ice cores collected October 2022 and April 2023. Vertical columns indicate ice facies types and changes with depth. Geochemical results are illustrated with cumulative horizontal bars adjacent to sampling depth (exact depth range indicated by black brackets). TDS in given in mg L^{-1} (upper bar; note unique charge range for each core) and the proportions cations (middle bar plot, Ca^{2+}, K^{+}, Mg^{2+}, and Na^{+}) and anions (lower bar plot, Cl^{-}, SO_4^{2-}, NO_3^{-}, and HCO_3^{-}).

https://doi.org/10.5194/egusphere-2026-2131
Preprint. Discussion started: 28 April 2026

4.4. Stable water isotopes

Isotopic compositions ($\delta^{18}O$ and δD) reveal that accreted ice samples generally have slightly higher $\delta^{18}O$ and δD values (Fig. 10a; -21±1.7 ‰) compared to naled ice (Fig. 10a; 24±2.3 ‰). Surface glacier ice plots separately from all naled samples with the lowest $\delta^{18}O$ value (-33.5 ‰), indicating the naled ice is distinctly different in water source and/or formation mechanism than surface glacier ice (Fig. 10a). Deuterium excess (*D-excess* = $\delta^2H - 8 \cdot \delta^{18}O$) values were used to determine the role of evaporation or freezing processes on the water samples isotopic composition (Fig. 10b). Deuterium excess values range from approximately 3 ‰ to 32 ‰ with a general trend of decreasing deuterium excess with increasing $\delta^{18}O$ values (Fig. 11).

Isotopic composition changes were also observed down-cores revealing potential freezing mechanisms. Within naled core I8 (Fig. 10b) $\delta^{18}O$ values generally decrease downcore (the lowest values detected at 132-146 cm of -29.5 ‰) and deuterium excess increasing from 9.8 ‰ at the top of the core to 25 ‰ at the base, exhibiting increasing fractionation processes downcore (Fig. 10b). However, a distinct but small increases in $\delta^{18}O$ and decreases in deuterium excess values are also seen at 104-108 cm mid-core. When plotted on a freezing curve naled ice samples I5, I8, I10 and I11 all display R^2 values of >0.9 suggesting sequential freezing downcore (Fig. 11). However, some core sections (in I2, I3, I4, I6, I7 and I9) do plot away from the freezing line with R^2 values of 0.07-0.93 (Fig. S4 in Supplementary Information). These sections are representative of discrete intervals of an increase in $\delta^{18}O$ and decreases in deuterium excess (also seen in Fig.10b) suggesting the start of new freezing packages.

https://doi.org/10.5194/egusphere-2026-2131
Preprint. Discussion started: 28 April 2026

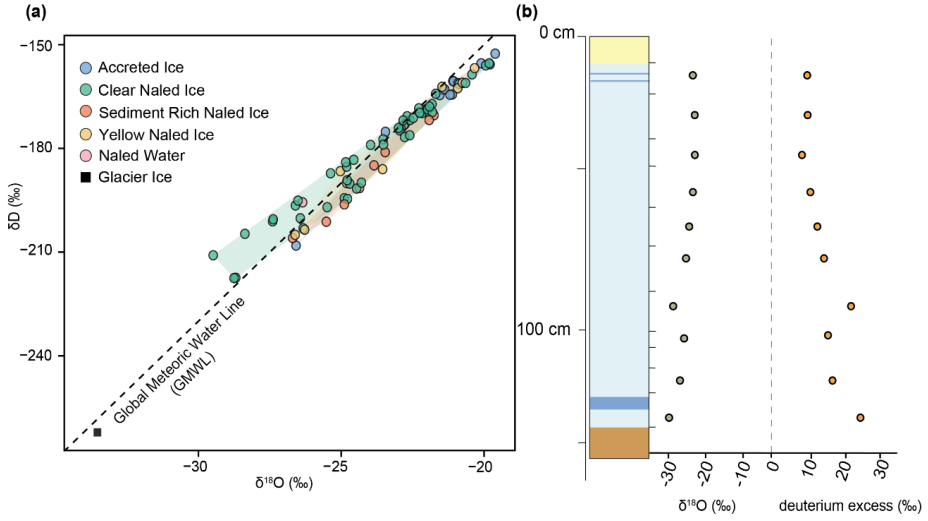

414

415 **Figure 10** Summary of stable isotope analysis of different ice types. (a) Cross-plot of δD
416 vs $\delta^{18}O$ compared to the Global Meteoric Water Line (GMWL). (b) Down-core change
417 in $\delta^{18}O$ (green points) and deuterium excess (orange points) in naled core I8. Shaded
418 regions in a-c denote the range of isotope and chemical data for ice and water. Note, a
419 select number of samples were analysed for stable water isotopes.

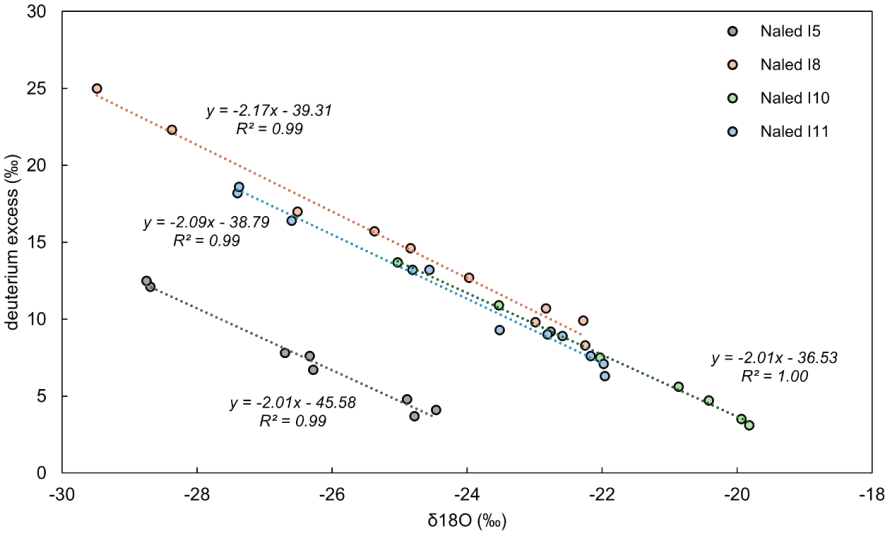

420

421 **Figure 11** Cross-plot of deuterium excess vs $\delta^{18}O$ of naled ice samples I5, I8, I10 and I11
422 on hypothesised freezing curves. All samples plot along the freezing curve in depth order
423 with increasing $\delta^{18}O$ and decreasing deuterium excess values at depth indicative of
424 sequential freezing downcore.

https://doi.org/10.5194/egusphere-2026-2131
Preprint. Discussion started: 28 April 2026

4.5. Electrical Resistivity Tomography

Electrical Resistivity Tomography (ERT) experiments were conducted <400 m from the terminus of Isunnguata Sermia, in an area where gravel-rich sediments dominate (Fig. 2). Our ERT images (Fig. 12) reveal considerable spatial heterogeneity in subsurface resistivity, spanning from $\log_{10}\rho$ ~0.83 to >8.1. In both ERT profiles, the uppermost layer (~1 - 5 m below the surface) is dominated by high resistivity values ($\log_{10}\rho$ >10.5), which are often indicative of dry and (at least partially) frozen material (Kneisel et al., 2014). As the surface is dominated by unsaturated gravel-rich glacial outwash material and compacted till, we expect this uppermost subsurface layer is similar in character.

Beneath this high resistivity layer, an intermediate zone (approximately 5–15 m below ground level) exhibits markedly lower resistivities ($\log_{10}\rho$ ~2 - 4), with resistivity varying across both profiles (yellow/white/blue colours in Fig. 12a). Bound by higher resistivity above and below, this zone likely represents a saturated sediment zone composed of sands/gravel and/or finer material or fractured bedrock (Palacky, 1987; Hauck & Kneisel, 2008; Reynolds 2011). Each of these materials can host groundwater, ice or subglacial meltwater. Localised zones of even lower resistivity ($\log_{10}\rho$ ~1- 2) are observed within this intermediate zone in both profiles (Fig. 12a, insets). Their geometry is suggestive of discrete pockets or conduits of moisture, potentially reflecting melting permafrost or glacial outflow pathways (e.g., Hauck & Kneisel, 2008). In both profiles, resistivity values abruptly return to $\log_{10}\rho$ ~10.5 and then $\log_{10}\rho$ ~10.6 Ωm beneath the intermediate zone. We interpret this to represent drier sediments, and/or frozen ground/ice (Kneisel et al., 2014), which we deem likely in the forefield of Isunnguata Sermia in winter.

https://doi.org/10.5194/egusphere-2026-2131
Preprint. Discussion started: 28 April 2026

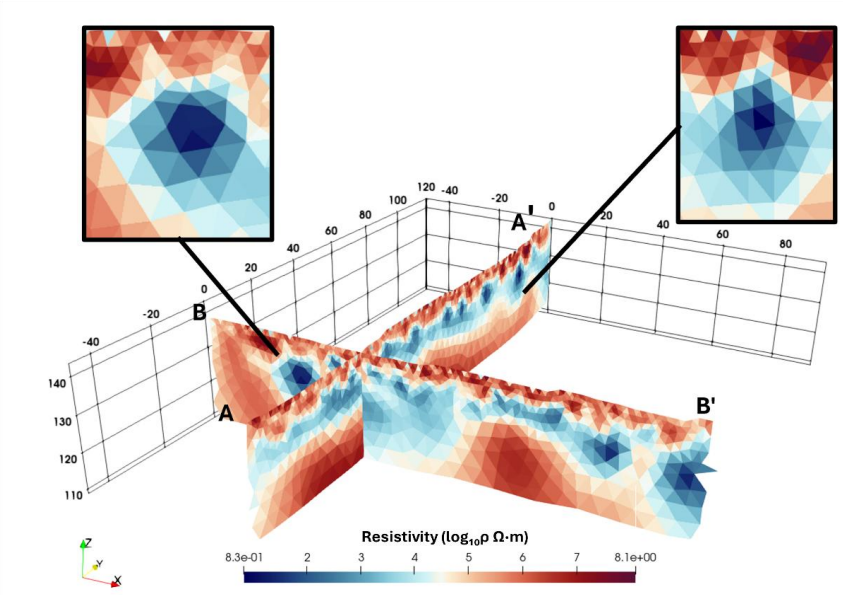

Figure 12 Two intersecting Electrical Resistivity Tomography (ERT) profiles surveyed in front of Isunnguata Sermia (location mapped on Figure 1). Depth and distance from starting location in metres. Resistivity values span a wide range (from $\log_{10}\rho$ ~1 to over 10.8), suggesting significant variations in moisture and/or porosity and/or liquid/frozen contrasts. Pockets of low resistivity, typical of high porosity or water-rich sediment zones are shown in highlighted boxes.

5. Discussion

5.1. Naled ice formation mechanisms

Time lapse camera footage, along with geochemical analyses of naledi and geophysical investigations of the glacial foreland at Isunnguata Sermia have allowed us to capture naledi structures in unprecedented detail. Our data show icings forming under both confined and unconfined water input conditions.

In the confined condition ice layers build up into dome-like structures, fed by the upwelling of waters from below (Fig. 5, 13). The waters likely originate from subglacial sources and are transported through subsurface conduits and/or saturated till (Fig. 12). In April 2024, naled ice domes were observed to have started forming overnight suggesting

https://doi.org/10.5194/egusphere-2026-2131
Preprint. Discussion started: 28 April 2026

that they may form relatively quickly (Fig. 5e). Following formation of an ice layer that restricts water flow, resultant build-up of water pressure beneath the naled can fracture the ice surface (e.g. Fig. 5c). The method of formation we describe here is akin to the formation mechanism described by Wadham et al., 2000 and Stachnik et al., 2016 (outlined in Fig. 1d-f).

Not all of the naledi studied were exclusively fed from waters below, and our results show that more than one formation mechanism exists. Automatic camera footage in Figure 5 shows that naledi can also be built from unconfined waters, as ice layers accumulate from overland water flow (beside upwellings) and from local precipitation such as the snow event captured in the automatic cameras (Fig. 13). These camera-derived observations, combined with geochemical analysis help to explain some of the unique ice facies we observed in the naled ice cores.

The waters with relatively high concentrations of TDS at the base of the naled cores are interpreted to reflect prolonged water storage in the subglacial system (at least over the winter months) - where chemical equilibration and mineral dissolution result in the highest TDS concentrations across our study site (e.g., Gokhman et al., 1987; Hodgkins et al., 2004; Stachnik et al., 2016; Yde et al., 2012). Layers of similar colours and geochemical signatures are also found within the naled cores such as I2, I8 and I10, suggestive of an eruptive process injecting these TDS-rich yellow coloured waters into the ice structure. Our geophysical analysis of the substrate supports both of these ideas, as low resistivity TMS returns are suggestive of a saturated sediment layer which could be fed by subglacial meltwaters and/or groundwater. The geophysical survey data interpretation also identifies a potential conduit for water flow (~ 5 m in diameter), which could efficiently transport subsurface waters over wintertime when air temperatures limit overland flow.

https://doi.org/10.5194/egusphere-2026-2131
Preprint. Discussion started: 28 April 2026

The clear naled ice with low solute concentrations suggest water origins from waters with limited mineral surfaces for reactions to occur on (such as supra- or englacial melt/storage and/or overwinter precipitation). These low solute waters form naled ice through relatively fast source to sink flow fed by proglacial meltwaters that haven't been transported through glacial till. An alternative explanation is that these layers, most often at the top of the naled cores are from only partially frozen (or partially wasted) ice/slush, with the ice retaining only some of the solutes and the rest of the solutes either running off (if unconfined) or being concentrated in the bottom layer of the freezing package. For example, in I8 we see very low TDS values (0.8-1.2 mg L^{-1}) in the middle of the core, followed by 15-141 mg L^{-1} further down the core and within the most isotopically enriched layers.

The downcore chemical and isotopic variation in naled ice can be explained, at least in part, by freezing processes. During freezing, heavier isotopes freeze first, with a stronger effect on ^{2}H than ^{18}O. Remaining, freezing water will fractionate on a freezing slope unlike that of meteoric water, controlled by the initial composition of the water and the fractionation factors of freezing (Jouzel and Souchez, 1982; Souchez and Jouzel, 1984). In a package of ice that froze in a single outburst event, we expect the heaviest isotopes on the top and lighter isotopes downcore. We also expect the concentration of dissolved solutes to significantly increase at the bottom of a freezing package, from the effects of progressive freeze concentration of dissolved solutes in the source water (Halde, 1980).

https://doi.org/10.5194/egusphere-2026-2131
Preprint. Discussion started: 28 April 2026

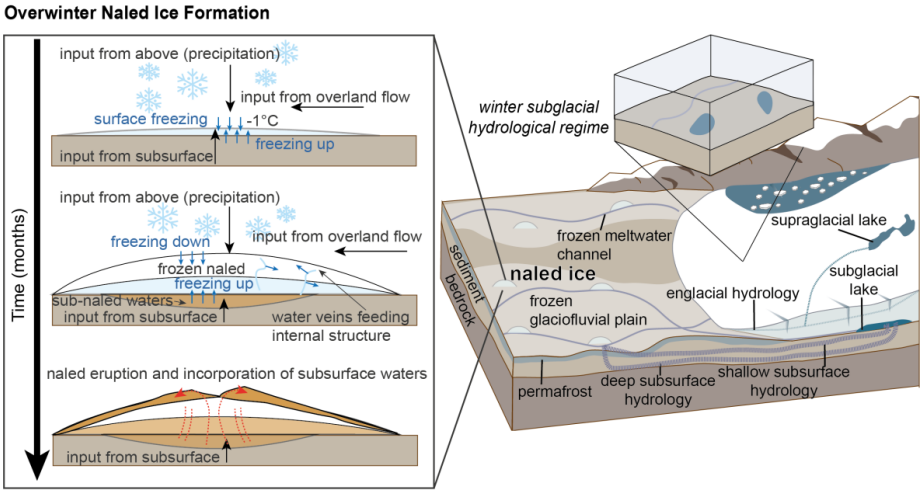

Figure 13. Conceptual diagram of naled ice formation mechanisms in western Greenland, based on ice facies, geochemical evidence and geophysical surveys of the proglacial area in front of Isunnguata Sermia. Inset box shows the evolution of naledi through winter, where water with long subsurface residence times discharge into the proglacial forefield. Other water sources, such as supraglacial and englacial melt, also contribute to naled ice layers freezing-in sequences. Naledi in this area incorporate both bottom-up and top-down formation mechanisms – incorporating two existing theories of naled formation. Water upwellings accrete onto the underside of the naled ice, and overland flow from supraglacial melt, englacial melt and precipitation accrete on top of the ice, where layers of either water flow can build up over time (through the winter).

The stable water isotopes analysed here reveal sequential freezing downcore with discrete freezing packages likely resulting from multiple upwelling events freezing on at the base of existing ice, pushing up into that existing ice, and creating domed structures over wintertime. However, we also observe that in the top sections of some samples of the longer cores (I2 and I7) and the shorter cores below 50 cm (I3, I4, I6 and I9) don't plot on this freezing curve line. This is suggestive of a different freezing sequence, potentially forming from a top-down process.

As water discharge is reduced over these winter months, and less capable of transporting glacial sediments, the naled ice is less sediment-laden than summer accreted ice formations which form under faster water flow conditions (Fig. 13). We therefore

https://doi.org/10.5194/egusphere-2026-2131
Preprint. Discussion started: 28 April 2026

conclude that the naledi on the forefield of Isunnguata Sermia form through a combination of unconfined and confined water sources. Subsurface waters which emerge through the substrate overlain by ice accumulate by freeze on below, whereas water flows and precipitation accumulate progressively upward (Fig. 13).

5.2. Accreted ice formation mechanisms

The formation of accreted ice was captured on automatic cameras in the late melt season September-October 2023 after a large upwelling event (Fig. 6). Based on the speed of their formation captured on cameras and supported by our geochemical analyses, we propose that they form where supercooled meltwater is evacuated into the glacier forefield and quickly freezes to form accreted ice during large eruption events during periods with cold surface temperatures creating structures composed of a mix of frazil ice and silt to fine sand sediments (Fig. 14). The ice accretions formed by the late melt season were observed to have persisted through the winter months preserved by cold temperatures, with gradual wastage evidenced by deflation and erosion of the ice surface over the winter (likely due to discrete melt events), leaving behind large amounts of sediment accumulations. Due to our focus on overwinter ice accumulations, we were not present in the summer months to observe the complete wastage of accreted ice, however due to repeated field visits, accreted ice structures were observed to have formed in the same locations in subsequent years. This observation indicates that the subsurface plumbing system is stable on interannual timescales.

The accreted ice samples exhibit a moderately uniform geochemical signature throughout, where the cores are dominated by sediment rich ice layers. This uniformity between sites, and within each core suggests consistent water sources, potentially derived from single or time-constrained outflow events. These cores are also geochemically

https://doi.org/10.5194/egusphere-2026-2131
Preprint. Discussion started: 28 April 2026

similar to previously characterised summer outflow waters in other studies (i.e., Graly et al., 2014; Graly et al., 2017a).

The subglacial hydrological system in this region is thought to provide fast-moving, highly pressurised subglacial waters into the proglacial field – generating large upwellings which gush up to several metres in heigh during summer months (Graly et al., 2017a). This water is presumably routed through the deep subglacial trough beneath Isunnguata Sermia (Lindbäck et al., 2015), where water will accumulate and interact with sediments and bedrock, before being driven up the reverse bed slope by high water pressure (when the subglacial hydrological system reaches capacity) (Cook et al., 2006; Lindbäck et al., 2014). The subsurface here is likely to be very high porosity sand/gravel deposited during the Holocene ice margin retreat and which favors 'groundwater' flow and not channelized flow. These highly pressurised supercooled waters then freeze into large icing structures close to minimal meltwater output zones at the glacier terminus (Fig. 6, 14). Currently, the growth and wastage rates of this accreted ice formation is unknown, however we observed that sporadic hours to days-long upwelling events contribute to the majority of the ice formation (Fig. 6a-c). We hypothesise, based on the results presented here that the formation timescale is likely fast with sudden upwellings of high velocity, highly pressurised waters erupt into the glacial forefield (Fig. 14).

https://doi.org/10.5194/egusphere-2026-2131
Preprint. Discussion started: 28 April 2026

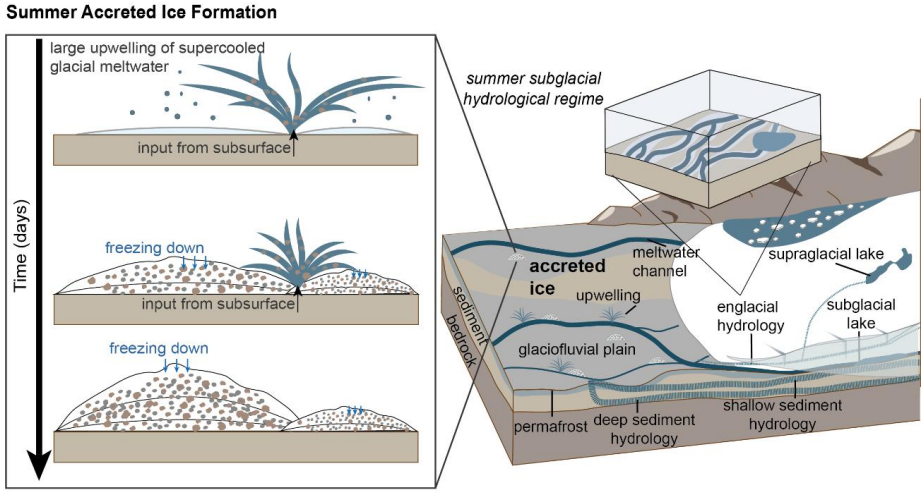

Figure 14 Conceptual diagram of accreted ice formation mechanisms in front of Isunnguata Sermia, Greenland, based on ice facies, geochemical evidence and geophysical surveys of the glacier foreland. Over summer, an efficient subglacial hydrological system moves sediment-loaded waters with low ion concentrations through subsurface water flow pathways. This allows accreted ice to form where upwellings of highly pressurised supercooled waters erupt into the forefield and freeze adjacent to the upwelling in an isolated event (see development of accreted ice structures in the inset panel).

5.3. Implications and comparisons with existing formation theories

Previous theories of naled formation have adapted either a top-down or bottom-up approach (Fig. 1). One approach details growth from waters below icing structures, with liquid water conduits within naled ice providing transport pathways insulated from the cold surface (Fig. 1f) (Stachnik et al., 2016; Wadham et al., 2000). The other approach focusses on accumulations from above where the cold winter atmosphere acts as a heat sink, freezing any waters or precipitation that accumulate from above (Fig. 1a-c) (Schohl and Ettema, 1986; Yde et al., 2012). Our observations and results supports both of these existing theories. Winter-forming naledi at our study site in Greenland form through a combination of top-down and bottom-up freezing processes, whilst summer accreted ice structures form by freeze-on of higher velocity, supercooled waters erupting onto the glacier foreland when surface temperatures are cold.

https://doi.org/10.5194/egusphere-2026-2131
Preprint. Discussion started: 28 April 2026

These systems offer insight into hydrological systems in Greenland that are difficult to ascertain from other means. They also show how water routing can vary spatially and temporally through the melt season. Geochemical differences in ice samples also raise important questions related to nutrient supply and TDS release from the Greenland Ice Sheet. With pronounced peaks in TDS detected in the overwinter naled waters, year round analyses of glacial waters is critical for capturing the full extent of foreland water flow and the impact of these waters on downstream ecosystems. Indeed, the seasonal changes in geochemistry we observe suggest that nutrient export in winter may be under-represented in existing literature, with important implications for our understanding of biogeochemical processes and their wider ecosystem downstream (Hawkings et al., 2025).

6. Conclusions

Previous research on proglacial icings, primarily on Svalbard, have proposed distinct formation mechanisms for the generation of winter naled ice structures. Over the course of four field seasons we have investigated the formation and build-up of winter-forming naledi and summer forming accreted ice together for the first time, at the proglacial forefield of Isunnguata Sermia in Greenland. Using 15 ice cores we geochemically characterised these ice structures for major ion and trace element concentrations, as well as $\delta^{2}H$ and $\delta^{18}O$ isotopic composition. By combining geochemistry with geophysical surveys and automatic camera footage, we can fully characterise and interpret icings, and the hydrological pathways that drive their formation at Isunnguata Sermia for the first time. The different geochemical signatures and the stratification of ice layers in the naled cores we extracted and analysed suggest that there are multiple water sources and pathways which contribute to naled formation at Isunnguata Sermia. We detected several distinct water types within the naledi, from highly concentrated naled bottom waters -

https://doi.org/10.5194/egusphere-2026-2131
Preprint. Discussion started: 28 April 2026

enriched in dissolved ions (originating from deep hydrological sources and/or groundwater), through to extremely dilute naled ice layers that most likely originate from supraglacial or englacial waters (which have had limited time and/or opportunity for sediment-water interaction). Our findings demonstrate how naledi can form through a combination of top-down and bottom-up freeze-on processes, where water is supplied from a variety of water sources. We suspect that similar mechanisms will create naledi elsewhere, though one process may dominate over another depending on local conditions (e.g. ice/bed topography, meltwater availability, ground conditions). In contrast, the summer accreted ice we observe at Isunnguata Sermia is much less geographically diverse, implying supercooled waters from the same (or similar) sources freeze-on quickly, presumably during more discrete, high output events. By analysing icings year round, we record a clear hydrological transition at Isunnguata Sermia, between summer (where supercooled waters emerge from efficient channelised drainage systems at pressure), and winter (where more inefficient distributed drainage networks dominate). . These seasonal changes drive different geochemical and nutrient outputs from water flows of the Greenland Ice Sheet, which can inform us about inland conditions which are hard to obtain through other means. Our observations are critical for evaluating glacier meltwater contributions to proglacial groundwater systems and downstream ecosystems, quantifying the seasonality associated with changes in solute availability and flux.

Data Availability

Supplementary information including all geochemical and isotope data and automatic camera GIFs are available at OSF doi: https://doi.org/10.17605/OSF.IO/A4QZK. Photographs of individual ice cores and detailed methodologies are provided alongside this manuscript.

https://doi.org/10.5194/egusphere-2026-2131
Preprint. Discussion started: 28 April 2026

Author Contributions

Conceptualisation – JG, KW, WPG, TLH, KL

Data Curation – RM, JG, CLH, KW, WPG, TLH, MJ, JRH, FN, AMR, MT, TMT, KW, BK, SM, HB, TK, AM, KL

Formal Analysis – RM, JG, KW, FN, MT, TMT, BK, SM, HB

Funding Acquisition – JG, KW, WPG, TLH, KL

Investigation – RM, JG, CLH, KW, WPG, TLH, MJ, JRH, FN, AMR, MT, TMT, KW, BK, SM, HB, TK, AM, KL

Methodology – RM, JG, KW, FN, MT, TMT, BK, SM, HB

Visualisation – RM, JG, KW, FN, MT, BK

Writing Original Draft – RM, JG, KW, FN

Writing Review and Editing – RM, JG, CLH, KW, WPG, TLH, MJ, JRH, FN, AMR, MT, TMT, KW, BK, SM, HB, TK, AM, KL

Competing Interests

The authors declare that they have no conflict of interest.

Acknowledgements

This work was funded by NSF-NERC grant OPP-2039854 and NE/W004860/1. The authors would like to acknowledge the support of Kangerlussuaq International Science Support (KISS), the Polar Geospatial Center for satellite imagery, and Peter Braddock for field safety support. The authors would also like to acknowledge Northumbria University's parental leave scheme, which provided research funding cover for KW.

References

Alley, R. B., Lawson, D. E., Evenson, E. B., Strasser, J. C., and Larson, G. J.: Glaciohydraulic supercooling: a freeze-on mechanism to create stratified, debris-rich

https://doi.org/10.5194/egusphere-2026-2131
Preprint. Discussion started: 28 April 2026

basal ice: II. Theory, Journal of Glaciology, 44, 563-569, 10.3189/S0022143000002070, 1998.

Bartholomew, I., Nienow, P., Sole, A., Mair, D., Cowton, T., Palmer, S., and Wadham, J.: Supraglacial forcing of subglacial drainage in the ablation zone of the Greenland ice sheet, Geophysical Research Letters, 38, 8, 10.1029/2011GL047063, 2011a.

Bhatia, M. P., Das, S. B., Xu, L., Charette, M. A., Wadham, J. L., and Kujawinski, E. B.: Organic carbon export from the Greenland ice sheet, Geochimica et Cosmochimica Acta, 109, 329-344, 10.1016/j.gca.2013.02.006, 2013.

Blanchy, G., Saneiyan, S., Boyd, J., McLachlan, P., and Binley, A.: ResIPy, an intuitive open source software for complex geoelectrical inversion/modeling, Computers & Geosciences, 137, 104423, 10.1016/j.cageo.2020.104423, 2020.

Carey, K. L.: Icings developed from surface water and ground water, 1973.

Chandler, D. M., Wadham, J. L., Lis, G. P., Cowton, T., Sole, A., Bartholomew, I., Telling, J., Nienow, P., Bagshaw, E. B., Mair, D., Vinen, S., and Hubbard, A.: Evolution of the subglacial drainage system beneath the Greenland Ice Sheet revealed by tracers, Nature Geoscience, 6, 195-198, 10.1038/NGEO1737, 2013.

Chu, W., Schroeder, D. M., Seroussi, H., Creyts, T. T., Palmer, S. J., and Bell, R. E.: Extensive winter subglacial water storage beneath the Greenland Ice Sheet, Geophysical Research Letters, 43, 12-484, 10.1002/2016GL071538, 2016.

Cook, S. J., Waller, R. I., Knight, P. G., and Simon J. Cook, R. I. W., Peter G. Knight: Glaciohydraulic supercooling: the process and its significance, Progress in Physical Geography, 30, 577-588, 10.1177/0309133306071141, 2006.

Evenson, E. B., Lawson, D. E., Strasser, J. C., Larson, G. J., Alley, R. B., Ensminger, S. L., and Stevenson, W. E.: Field evidence for the recognition of glaciohydrologic supercooling, Glacial Processes Past and Present, 10.1130/0-8137-2337-X.23, 1999.

https://doi.org/10.5194/egusphere-2026-2131
Preprint. Discussion started: 28 April 2026

695 Gokhman, V. V., Gokhman, V. V., and Gokhman, V. V.: Distribution and conditions of
696 formation of glacial icings on Spitsbergen, Polar Geography, 249-260,
697 10.1080/10889378709377334, 1987.
698 Graly, J., Harrington, J., and Humphrey, N.: Combined diurnal variations of discharge
699 and hydrochemistry of the Isunnguata Sermia outlet, Greenland Ice Sheet, The
700 Cryosphere, 11, 1131-1140, 10.5194/tc-11-1131-2017, 2017a.
701 Graly, J. A., Drever, J. I., and Humphrey, N. F.: Calculating the balance between
702 atmospheric CO2 drawdown and organic carbon oxidation in subglacial hydrochemical
703 systems, Global Biogeochemical Cycles, 31, 709-727, 10.1002/2016GB005425, 2017b.
704 Graly, J. A., Humphrey, N. F., and Harper, J. T.: Chemical depletion of sediment under
705 the Greenland Ice Sheet, Earth Surface Processes and Landforms, 41, 1922-1936,
706 10.1002/esp.3960, 2016.
707 Graly, J. A., Humphrey, N. F., and Licht, K. J.: Two Metrics Describing the Causes of
708 Seasonal and Spatial Changes in Subglacial Aqueous Chemistry, Frontiers in Earth
709 Science, 6, 195, 10.3389/feart.2018.00195, 2018.
710 Halde, R.: Concentration of impurities by progressive freezing, Water Research 14, 575-
711 580, 10.1016/0043-1354(80)90115-3, 1980
712 Harden, D., Barnes, P., and Reimnitz, E.: Distribution and Character of Naleds in
713 Northeastern Alaska, Arctic, 30, 28-40, 1977.
714 Hauck, C. and Kneisel, C.: *Applied geophysics in periglacial environments* (Vol. 10).
715 Cambridge University Press, 2008.
716 Hawkings, J.R., Bradley, J.A., Doting, E.L., Hassan, N., Hendry, K.R., Holt, A.D., Hood,
717 E., Spencer, R.G., Stibal, M., Tranter, M. and Venturelli, R.A.: Glacier biogeochemical
718 cycling and downstream impacts. *Nature Reviews Earth & Environment*, 1-20,
719 10.1038/s43017-025-00751-1, 2025.

https://doi.org/10.5194/egusphere-2026-2131
Preprint. Discussion started: 28 April 2026

720 Hawkings, J., Wadham, J., Tranter, M., Telling, J., Bagshaw, E., Beaton, A., Simmons,
721 S.-L., Chandler, D., Tedstone, A., and Nienow, P.: The Greenland Ice Sheet as a hot spot
722 of phosphorus weathering and export in the Arctic, Global Biogeochemical Cycles, 30,
723 191-210, 191-210, 10.1002/2015GB005237, 2016.
724 Hodgkins, R., Tranter, M., and Dowdeswell, J. A.: The Characteristics and Formation of
725 A High-Arctic Proglacial Icing, Geografiska Annaler Series A-physical Geography,
726 86(3), 265-275, 10.1111/j.0435-3676.2004.00230.x, 2004.
727 Jouzel, J. and Souchez, R. A.: Melting–Refreezing at the Glacier Sole and the Isotopic
728 Composition of the Ice, Journal of Glaciology, 28, 35-42, 10.3189/S0022143000011771,
729 1982.
730 Kane, D. L.: Physical mechanics of aufeis growth, Canadian Journal of Civil Engineering,
731 8, 186-195, 1981.
732 Kneisel, C., Emmert, A. and Kästl, J.: Application of 3D electrical resistivity imaging for
733 mapping frozen ground conditions exemplified by three case
734 studies. *Geomorphology*, *210*, 71-82, 10.1016/j.geomorph.2013.12.022, 2014
735 Krawczyk, W.E., Lefauconnier, B. and Pettersson, L.E.: Chemical denudation rates in the
736 Bayelva catchment, Svalbard, in the fall of 2000. *Physics and Chemistry of the Earth,*
737 *Parts A/B/C*, *28*(28-32), 1257-1271, 10.1016/j.pce.2003.08.054, 2003.
738 Lawson, D. E., Strasser, J. C., Evenson, E. B., Alley, R. B., Larson, G. J., and Arcone, S.
739 A.: Glaciohydraulic supercooling: a freeze-on mechanism to create stratified, debris-rich
740 basal ice: I. Field evidence, Journal of Glaciology, 44, 547-562,
741 10.3189/S0022143000002069, 1998.
742 Lawson, E. C., Wadham, J. L., Tranter, M., Stibal, M., Lis, G. P., Butler, C. E. H.,
743 Laybourn-Parry, J., Nienow, P., Chandler, D., and Dewsbury, P.: Greenland Ice Sheet

https://doi.org/10.5194/egusphere-2026-2131
Preprint. Discussion started: 28 April 2026

744 exports labile organic carbon to the Arctic oceans, Biogeosciences, 11, 4015-4028,
745 10.5194/bg-11-4015-2014, 2014.
746 Lindbäck, K., Pettersson, R., Hubbard, A. L., Doyle, S. H., As, D., Mikkelsen, A. B., and
747 Fitzpatrick, A. A.: Subglacial water drainage, storage, and piracy beneath the Greenland
748 ice sheet, Geophysical Research Letters, 42, 7606-7614, 10.1002/2015GL065393, 2015.
749 Lindbäck, K., Pettersson, R., Doyle, S. H., Helanow, C., Jansson, P., Kristensen, S. S.,
750 Stenseng, L., Forsberg, R., and Hubbard, A. L.: High-resolution ice thickness and bed
751 topography of a land-terminating section of the Greenland Ice Sheet, Earth System
752 Science Data, 6, 331-338, 10.5194/essd-6-331-2014, 2014.
753 Livingstone S., Storrar R., Doyle S., Thorpe S., Moffatt A., Sole A., Chudley T. R.,
754 Gimbert F., Graly J., Licht K., Winter K., Jayarapu, A., Bagshaw, E., Barruol, G., Bauer,
755 K., Bianchi, G., Buzzard, S., Clason, C., Craw, L., Davison, B., Edwards, L., Gilhooly,
756 W., Hamilton, T. L., Hansen, C., Hawkins, J., Ing, R., Jatta, M., Jones, A., Kennedy, T.,
757 Killingbeck, S., Le Bris, T., McCerery, R., Messerli, A., Michel, A., Napoleoni, F.,
758 Peacey, M., Prior-Jones, M. R., Ross, N., Veness, R., Hepburn, A., Booth, A. Ice
759 dynamic and hydrological response to ice-dammed lake drainages at Isunnguata Sermia,
760 West Greenland, Journal of Glaciology, 2026.
761 Livingstone, S. J., Sole, A. J., Storrar, R. D., Harrison, D., Ross, N., and Bowling, J.:
762 Brief communication: Subglacial Lake drainage beneath Isunguata Sermia, West
763 Greenland: geomorphic and ice dynamic effects, The Cryosphere, 13, 2789-2796,
764 10.5194/tc-13-2789-2019, 2019.
765 Mallinson, L., Swift, D. A., and Sole, A. J.: Proglacial icings as indicators of glacier
766 thermal regime: ice thickness changes and icing occurrence in Svalbard, Geografiska
767 Annaler Series A-physical Geography, 101(4), 334-349,
768 10.1080/04353676.2019.1670952, 2019.

https://doi.org/10.5194/egusphere-2026-2131
Preprint. Discussion started: 28 April 2026

769 Meierbachtol, T., Harper, J., and Humphrey, N.: Basal drainage system response to
770 increasing surface melt on the Greenland Ice Sheet, Science, 341, 777-779,
771 10.1126/science.1235905, 2013.
772 Meire, L., Meire, P., Struyf, E., Krawczyk, D. W., Arendt, K. E., Yde, J. C., Pedersen, T.
773 J., Hopwood, M. J., Rysgaard, S., and Meysman, F. J. R.: High export of dissolved silica
774 from the Greenland Ice Sheet, Geophysical Research Letters, 43, 9173-9182,
775 10.1002/2016GL070191, 2016.
776 Morse, P. D. and Wolfe, S. A.: Geological and meteorological controls on icing (aufeis)
777 dynamics (1985 to 2014) in subarctic Canada, Journal of Geophysical Research: Earth
778 Surface, 120, 1670-1686, 10.1002/2015JF003534, 2015.
779 Pain, A. J., Martin, J. B., Martin, E. E., Rennermalm, Å. K., and Rahman, S.:
780 Heterogeneous CO2 and CH4 content of glacial meltwater from the Greenland Ice Sheet
781 and implications for subglacial carbon processes, The Cryosphere, 15, 1-33, 10.5194/tc-
782 15-1627-2021, 2021.
783 Palacky, G.J.: Resistivity characteristics of geologic targets, In: Electromagnetic methods
784 in applied geophysics, 10.1190/1.9781560802631.ch3, 1987
785 Pitcher, L. H., Smith, L. C., Gleason, C. J., Miège, C., Ryan, J. C., Hagedorn, B., van As,
786 D., Chu, W., and Forster, R. R.: Direct observation of winter meltwater drainage from the
787 Greenland Ice Sheet, Geophysical Research Letters, 47, e2019GL086521,
788 10.1029/2019GL086521, 2020.
789 Reynolds, J.M.: An introduction to applied and environmental geophysics. John Wiley &
790 Sons., 2011
791 Roberts, M. J., Russell, A. J., Tweed, F. S., and Knudsen, Ó.: Controls on englacial
792 sediment deposition during the November 1996 jökulhlaup, Skeiðarárjökull, Iceland,
793 Earth Surface Processes and Landforms, 26, 935-952, 10.1002/esp.236, 2001.

https://doi.org/10.5194/egusphere-2026-2131
Preprint. Discussion started: 28 April 2026

794 Roberts, M. J., Tweed, F. S., Russell, A. J., Knudsen, O. s., Lawson, D. E., Larson, G. J.,
795 Evenson, E. B., and Björnsson, H.: Glaciohydraulic supercooling in Iceland, Geology,
796 30, 871-874, 10.1130/0091-7613(2002)030, 2002.
797 Schohl, G. A. and Ettema, R.: Theory and Laboratory Observations of Naled Ice Growth,
798 Journal of Glaciology, 32, 168-177, 10.3189/S0022143000015483, 1986.
799 Sobota, I.: Icings and their role as an important element of the cryosphere in High Arctic
800 glacier forefields, Bulletin of Geography: Physical Geography Series, 81-93,
801 10.1515/bgeo-2016-0006, 2016.
802 Sodemann, H., Mørkved, P. T., and Wahl, S.: FLIIMP - a community software for the
803 processing, calibration, and reporting of liquid water isotope measurements on cavity-
804 ring down spectrometers, MethodsX, 11, 102297, 10.1016/j.mex.2023.102297, 2023.
805 Souchez, R. A. and Jouzel, J.: On the Isotopic Composition in δD and δ18O of Water and
806 Ice During Freezing, Journal of Glaciology, 30, 369-372, 10.3189/S0022143000006249,
807 1984.
808 Stachnik, L., Yde, J. C., Kondracka, M., D., I., and Grzesik, M.: Glacier naled evolution
809 and relation to the subglacial drainage system based on water chemistry and GPR surveys
810 (Werenskioldbreen, SW Svalbard), Annals of Glaciology, 57, 19-30,
811 10.1017/aog.2016.9, 2016.
812 van Gool, J. A. M., Connelly, J. N., Marker, M., and Mengel, F. C.: The Nagssugtoqidian
813 Orogen of West Greenland: Tectonic evolution and regional correlations from a West
814 Greenland perspective, Canadian Journal of Earth Science, 39, 665-686, 10.1139/E02-
815 027, 2002.
816 Wadham, J. L., Tranter, M., and Dowdeswell, J. A.: Hydrochemistry of meltwaters
817 draining a polythermal-based, high-Arctic glacier, south Svalbard: II. Winter and early

https://doi.org/10.5194/egusphere-2026-2131
Preprint. Discussion started: 28 April 2026

818 Spring, Hydrological Processes, 14, 1767-1786, 10.1002/1099-
819 1085(200007)14:10<1767::aid-hyp103>3.0.co;2-q, 2000.
820 Wadham, J. L., Hawkings, J., Telling, J., Chandler, D., Alcock, J., O'Donnell, E., Kaur,
821 P., Bagshaw, E., Tranter, M., Tedstone, A., and Nienow, P.: Sources, cycling and export
822 of nitrogen on the Greenland Ice Sheet, Biogeosciences, 13, 6339-6352, 10.5194/bg-13-
823 6339-2016, 2016.
824 Weng, Y., Touzeau, A. and Sodemann, H.: Correcting the impact of the isotope
825 composition on the mixing ratio dependency of water vapour isotope measurements with
826 cavity ring-down spectrometers, Atmospheric Measurement Techniques, 13(6), 3167-
827 3190, 2020.
828 Yde, J. C., Knudsen, N. T., Hasholt, B., and Mikkelsen, A. B.: Meltwater chemistry and
829 solute export from a Greenland Ice Sheet catchment, Watson River, West Greenland,
830 Journal of Hydrology, 519, 2165-2179, 10.1016/j.jhydrol.2014.10.018, 2014.
831 Yde, J. C., Hodson, A. J., Solovjanova, I., Steffensen, J. P., Nørnberg, P., Heinemeier, J.,
832 and Olsen, J.: Chemical and isotopic characteristics of a glacier-derived naled in front of
833 Austre Grønfjordbreen, Svalbard, Polar Research, 31, 17628, 10.3402/polar.v31i0.17628,
834 2012.
835 Yoshikawa, K., Hinzman, L. D., and Kane, D. L.: Spring and aufeis (icing) hydrology in
836 Brooks Range, Alaska, Journal of Geophysical Research: Biogeosciences, 112(G4),
837 10.1029/2006JG000294, 2007.